Appl. Phys. A (2017) 123:355
DOI 10.1007/s00339-017-0972-8

Applied Physics A
Materials Science & Processing

Effect of S^{2-} donors on synthesizing and photocatalytic degrading properties of ZnS/RGO nanocomposite

Yanli Qin[1,2] · Zheng Sun[1,2] · Wenwen Zhao[1,2] · Zhenyu Liu[1] · Dingrui Ni[1] · Zongyi Ma[1]

Received: 3 January 2017 / Accepted: 11 April 2017 / Published online: 17 April 2017

Abstract To synthesize ZnS/RGO nanocomposite via one-step solvothermal method with graphene oxide (GO) aqueous solution as precursor, we selected sodium sulfide and thiourea as S^{2-} donor, respectively, with the aim to evaluate the effect of different S^{2-} sources on the synthesis and degrading properties of the composite. The photocatalytic activity of the nanocomposite was investigated through the photocatalytic degradation of methylene blue in aqueous solution. Results showed that ZnS/RGO nanocomposites were synthesized using both sodium sulfide and thiourea as S^{2-} donor, respectively. Compared to pure ZnS, the nanocomposites exhibited higher photocatalytic activity; furthermore, the nanocomposite prepared with sodium sulfide as the S^{2-} source exhibited much better photocatalytic degradation efficiency than that with thiourea as the S^{2-} source. The surface reaction rate constant of the former was two times higher than that of the latter and was six times higher than that of pure ZnS sample.

✉ Dingrui Ni
drni@imr.ac.cn

✉ Zongyi Ma
zyma@imr.ac.cn

[1] Shenyang National Laboratory for Materials Science, Institute of Metal Research, Chinese Academy of Sciences, 72 Wenhua Road, Shenyang 110016, China

[2] School of Science, Shenyang Ligong University, No.6 Nanping Central Road, Shenyang 110159, China

1 Introduction

The optical catalyst of semiconductors has received much attention in the field of organic pollutant degradation, because these catalysts can convert light energy into chemical energy without regenerating pollution in the environment [1, 2]. Photocatalysts usually depend on the capability of semiconductor materials to absorb light and to produce photo-generated electronic e^- and hole h^+ under the excitation light condition. A series of redox reactions then occur with the adsorption of organic pollutant molecules on the surface of the catalyst to generate a degradation effect.

ZnS, a direct band gap semiconductor, exhibits strong oxidation and no secondary pollution. The photocatalytic reaction of ZnS can be catalyzed by ultraviolet (UV) light to degrade organic pollutants [3]. However, the photocatalytic efficiency of ZnS is not satisfactory owing to the fast recombination of photo-generated electron–hole pair. Some researches showed that combining the conventional photocatalyst with other materials can effectively reduce this recombination phenomenon, such as precious metals [4, 5], compound semiconductors [6, 7], and carbon nanotubes [8].

Graphene owns a 2D sp^2 carbon network and attracted much interest because of its unique electronic, mechanical, and thermal properties [9, 10]. Furthermore, the high carrier mobility, mechanical flexibility, optical transparency, and chemical stability of graphene generate much opportunity for the development of high-performance composites [11, 12]. Owing to this unique nanostructure, the photocatalytic performance of the graphene-composite catalyst can be improved; for example, researches on the development of loading ZnS with graphene have been

reported, which exhibited an improved photocatalytic property [13, 14].

For the preparation of ZnS nanoparticles via "One-step solvothermal method" which is one of the main techniques for preparing nanocomposites based on graphene, a single sulfur source was usually used as a reaction precursor. However, the hydrolysis rate of different reaction precursors may affect the morphology and surface distribution of the nanoparticles; for instance, the hydrolysis rate of sodium sulfide ($Na_2S{\cdot}9H_2O$, 186 g/L, 20 °C) is higher than that of thiourea ($SC(NH_2)_2$, 137 g/L, 20 °C). Therefore, it is important to elucidate the effect of different S^{2-} donors on the synthesis and photocatalytic degrading properties of ZnS nanocomposite.

In the current study, ZnS/RGO nanocomposites were synthesized via one-step solvothermal method with graphene oxide (GO) aqueous solution as precursor. $Na_2S{\cdot}9H_2O$ and $SC(NH_2)_2$ were considered as S^{2-} donor with the aim to evaluate the effect of different S^{2-} sources on the synthesizing and degrading properties of the nanocomposites. Furthermore, the photocatalytic performance of the composites prepared under different reaction conditions is evaluated using methylene blue (MB).

2 Experimental

2.1 Materials

GO aqueous solution (2 mg/mL) was purchased from the Shanxi Coal Research Institute, Chinese Academy of Sciences. $Zn(Ac)_2{\cdot}2H_2O$, $Na_2S{\cdot}9H_2O$, $SC(NH_2)_2$, MB, $(CH_2OH)_2$, and $C_6H_{14}O_4$ were purchased from Sinopharm Chemical Reagent Co., Ltd, and used without further purification. All laboratory reagents employed in the analysis were pure with deionized water being utilized in all experiments.

2.2 Preparation of ZnS–RGO nanocomposites

In a typical synthesis process, ZnS/RGO nanocomposites were prepared with the one-step solvothermal method using $(CH_2OH)_2$ as a solvent, along with $Na_2S{\cdot}9H_2O$ and $SC(NH_2)_2$ as two sulfur ion sources. As shown in Fig. 1, 110 mg of $Zn(Ac)_2{\cdot}2H_2O$ was first dissolved in 20 mL of $(CH_2OH)_2$. Then, 20 mL (2 mg/mL) GO aqueous solution was added into the solution and subjected to ultrasonic treatment for 30 min to produce a light brown solution. Subsequently, 120 mg of sodium sulfide and 38 mg of thiourea were added separately into 20 mL solvents under ultrasonic treatment. This solution was then added into the previously light brown solution and stirred for 30 min. Finally, the mixture was autoclaved in a Teflon-lined stainless steel vessel at 180 °C for 10 h. The reaction products were centrifuged and washed with deionized water and anhydrous ethanol; then, the products were dried in a vacuum oven at 60 °C.

2.3 Characterization

The phase and crystallite size of the ZnS/RGO composites were characterized with an automated X-ray diffractometer (XRD, Rigaku D/max 2400) with a monochromated CuKα radiation ($\lambda = 0.154056$ nm). The surface morphology, particle size, and composition of photocatalysts were examined using a transmission electron microscope (TEM, TECNAI 20). Raman spectra were detected by a Raman Spectrometer (Jobin–Yvon LabRAM, HR800). The UV–vis absorption spectrum was recorded with a UV–vis spectrophotometer (INESA, UV757CRT/PC).

2.4 Photocatalytic performance experiments

The photocatalytic activity levels of different composite photocatalysts were estimated by monitoring the degradation of MB in a self-assembled apparatus with a UV lamp (8 W) as the radiation source. Typically, 20 mg of photocatalysts is suspended in a beaker containing an aqueous solution that consists of model dye (50 mL; 20 mg/L) in the photocatalytic experiment. First, the suspension was subjected to ultrasonic treatment for 30 min to reach adsorption–desorption equilibrium without UV light exposure. Subsequently, a photocatalytic reaction was initiated by the exposure to UV light under continuous

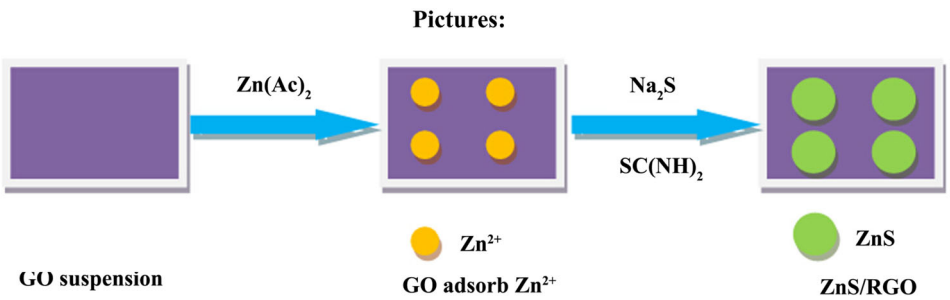

Fig. 1 Proposed scheme for ZnS/RGO fabricated processes

magnetic stirring. At specific time intervals, 3 mL suspensions were sampled, and centrifuged. Then, the supernatants were collected for analysis with the UV–vis absorption spectrometer.

The intensity of the maximum absorption peak (663 nm) of the MB dye was regarded as a measure of residual MB dye concentration. According to Lambert–Beer law, $C_t/C_0 = A_t/A_0$, where C_0 is the concentration of the MB solution after dark adsorption, C_t is the concentration of the MB solution after illumination time t, A_0 is the absorbance of the MB solution after dark adsorption, and A_t is the absorbance of the MB solution after illumination time t.

3 Results and discussion

3.1 Characterization of ZnS/RGO nanocomposites

Figure 2 depicts the representative XRD patterns of the ZnS/RGO nanocomposites with either sodium sulfide (ZnS/RGO-1, Fig. 2c) or thiourea (ZnS/RGO-2, Fig. 2d) as sulfur sources, and the XRD patterns of graphite (Fig. 2a, here for reference) and GO (Fig. 2b) are also provided for comparison. As shown in Fig. 2c and d, three strong peaks are detected at 2θ around 28.61°, 47.62°, and 56.51°; these peaks are assigned to the (111), (220), and (311) reflections of the face-centered cubic ZnS (JCPDS 05-0566), respectively. According to Scherrer's equation, the average size of ZnS nanoparticles is estimated to be 5–10 nm, which is in good agreement with the TEM observation, as shown in Fig. 3.

The crystallinity of the ZnS nanoparticles is similar to that of pure ZnS. By contrast, no characteristic peaks were assigned to GO (001) or graphite (003) in the nanocomposites. If the regular stacks of graphene are destroyed, such as by exfoliation, their diffraction peaks weaken or may even disappear [15]. The crystallinity of a sample is a key factor in the utilization of the photocatalytic properties

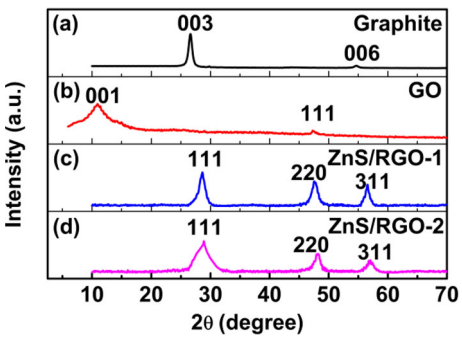

Fig. 2 Typical XRD patterns of ZnS/RGO nanocomposites with sodium sulfide (ZnS/RGO-1) and thiourea (ZnS/RGO-2) as sulfur sources

of the sample, and the better the crystallinity, the better the properties. It is seen that ZnS/RGO-1 showed stronger diffraction intensity and narrower full-width at half-maximum than ZnS/RGO-2, implying the better crystallinities.

Figure 3 presents the TEM images of the ZnS/RGO nanocomposites prepared with sodium sulfide and thiourea. ZnS nanoparticles were uniformly distributed on the surface of the graphene sheets, whose edge position was clearly distinguishable from the 2D structures displaying surface wrinkles. Such sheets play an important role in promoting the growth and surface distribution of ZnS nanoparticle, and the agglomeration phenomenon can be effectively prevented [16]. However, owing to the high concentration of graphene sheets in solution, a large number of tiny primary nanoparticles tended to condense and aggregate to form larger particles [17].

It can be seen that the ZnS nanoparticles of ZnS/RGO with sodium sulfide as S^{2-} donor (Fig. 3a) were distributed more uniformly than that with thiourea as S^{2-} donor (Fig. 3b). This may result from different hydrolysis rates of the two S^{2-} donors. It was reported that the hydrolysis rate of sodium sulfide is significantly higher than that of thiourea (186 vs. 137 g/L, 20 °C); hence, sodium sulfide can be hydrolyzed rapidly to produce S^{2-} during the reaction in hydrothermal synthesis. Then, S^{2-} ions combine to Zn^{2+} on the GO layer to generate zinc sulfide nuclei through the reaction, and many small, initial zinc sulfide nuclei condense on the surface to form ZnS nanoparticles.

Figure 4 exhibits the Raman spectra of the pristine graphite, GO, ZnS/RGO-1, and ZnS/RGO-2. The following observations can be made. First, the Raman spectrum of the pristine graphite, as expected, displays a prominent G peak as the only feature at 1583 cm^{-1} (Fig. 4a), corresponding to the first-order scattering of the E_{2g} mode [18]. Second, GO exhibits a G band shift to approximately 1589 cm^{-1} (Fig. 4b), which corresponds to an E_{2g} graphite mode related to the vibration of the sp^2-bonded carbon atoms in a 2D hexagonal lattice. Another dominant peak detected at roughly 1345 cm^{-1} (D band) is related to the defects and disorder in the hexagonal graphitic layers [19, 20]. Third, two typical peaks are observed on both the curves of ZnS/RGO-1 (Fig. 4c) and ZnS/RGO-2 (Fig. 4d). However, the typical peaks of the nanocomposites shift to different values as a result of the reduction of GO.

Compared with GO, the D band of ZnS/RGO nanocomposites is blue-shifted, while the G band showed a slight red shift. These shifts in the Raman spectra indicate that interactions existed between ZnS and graphene, and the interactions are not only beneficial to improving the stability but also favorable to enhancing the photocatalytic activity of ZnS [21]. The degree of disorder of the two nanocomposites can be derived from the intensity ratios of the D and G bands. As shown in Fig. 4, the ratio of ZnS/

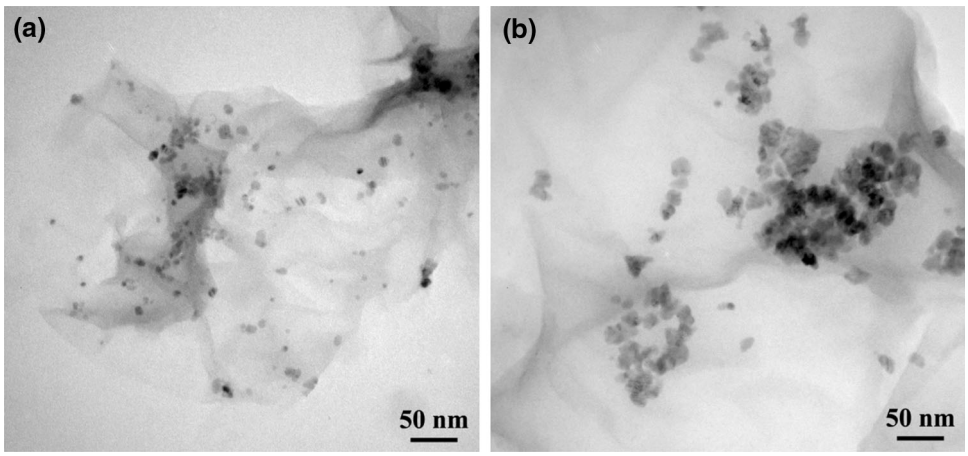

Fig. 3 TEM images of ZnS–RGO composites prepared with sodium sulfide (**a**) and thiourea (**b**) as sulfur sources

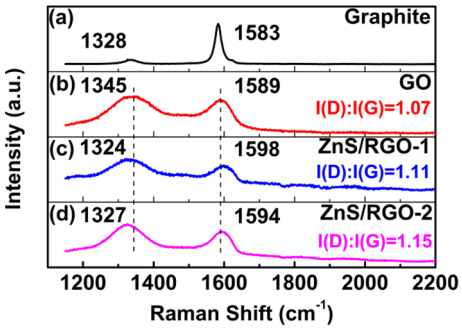

Fig. 4 Raman spectra of ZnS/RGO nanocomposites with sodium sulfide (ZnS/RGO-1) and thiourea (ZnS/RGO-2) as sulfur sources

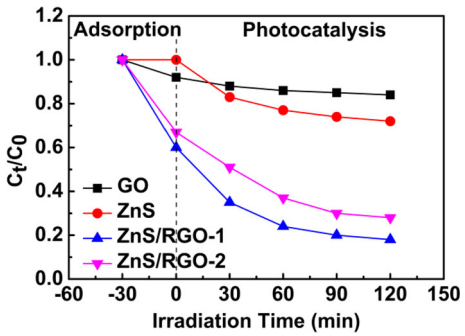

Fig. 5 Photocatalytic degradation curves of MB in the presence of ZnS and ZnS/RGO composites under UV light irradiation (ZnS/RGO-1 by sodium sulfide, ZnS/RGO-2 by thiourea)

RGO-1 is lower than that of ZnS/RGO-2. This result implies that the nanocomposite prepared with sodium sulfide as S^{2-} donor is less defective than that prepared with thiourea as S^{2-} donor [22].

3.2 Photocatalytic performance of ZnS/RGO nanocomposites

The photocatalytic properties of the ZnS/RGO nanocomposites prepared with different S^{2-} ion sources were evaluated based on the efficiency of MB photocatalytic degradation under UV irradiation (Fig. 5). It can be seen that pure graphene sample substantially exhibited no photocatalytic activity. The pure ZnS sample showed a certain photocatalytic activity. In contrast, the ZnS/RGO nanocomposites showed a significantly improved photocatalytic degradation efficiency. This indicates that the introduction of graphene into ZnS plays an important role in improving the photocatalytic performance. In addition, the photocatalytic degradation efficiency of ZnS/RGO-1 was higher than that of ZnS/RGO-2, and this may result from the higher hydrolysis rate of sodium sulfide than that of thiourea.

The photocatalytic degradation of organic dye molecules on the surface of the ZnS/RGO nanocomposites can be considered as two inseparable and mutually promoted processes. For one thing, contaminant molecules are adsorbed on the surface of graphene and this process will reach the adsorption equilibrium soon. However, the adsorption equilibrium will be destroyed due to the occurrence of the oxidation reaction which degrades the organic pollutants. Thus, the organic pollutant molecules would be continuously adsorbed on the surface of the composites and be photocatalytically degraded due to ultraviolet radiation effect. For another, the photo-generated electrons and holes can be effectively separated by graphene, and thus, the quantum yield is significantly improved. Photo-generated electrons and holes further react to generate a variety of active substances, and the organic dye molecules adsorbed on the surface of the nanocomposites are oxidatively degraded. Consequently, the nanocomposites show a significantly enhanced photocatalytic activity resulting from the synergistic effect of adsorption–photocatalytic degradation. It should be pointed out that for the improved photocatalytic degradation property of the composite, the enhancement of adsorption

capacity is just an influencing factor; however, the photocatalytic reaction of the composite itself is the main degrading mechanism.

Figure 6 shows the comparison diagram of surface reaction rate constant which can be expressed by the Langmuir–Hinshelwood model [23]. The photocatalytic degradation of MB by the nanocomposites under UV light obeyed pseudo-first-order kinetics with respect to the concentration of MB:

$$\ln\left(\frac{C_0}{C_t}\right) = k_c \times t \quad (1)$$

where k_c is the surface reaction rate constant, which is used as the basic kinetic parameter for different photocatalysts. The surface reaction rate constant values could be deduced from the linear fitting of $\ln(C_0/C_t)$ vs. t. The results show that k_c was enhanced by the introduction of graphene, and the surface reaction rate constant of ZnS/RGO-1 was two times higher than that of ZnS/RGO-1 and was six times higher than that of pure ZnS sample [24].

Recently, there are several reports in the synthesis and application of ZnS/RGO nanocomposites. Feng et al. [14] prepared a ZnS/RGO composite using a one-pot hydrothermal synthesis system, in which the pH value of solution was adjusted by the addition of ammonia solution. Sookhakian et al. [17] developed ZnS/RGO composites through a one-step solvothermal method without using templates or surfactants, resulting in improved photocatalytic degradation for MB. However, in these works, high power excitation light sources were required in the photocatalytic degradation experiments. In the present study, the same degradation effect was achieved using a small power excitation light source. Hence, it is urgent for us to synthesize ZnS/RGO nanocomposites with high-efficiency degradation under the condition of weak excitation light source.

Figure 7 illustrates the photocatalytic degradation mechanism of organic dyes by the semiconductor catalyst under UV light irradiation. Based on the excitation of the

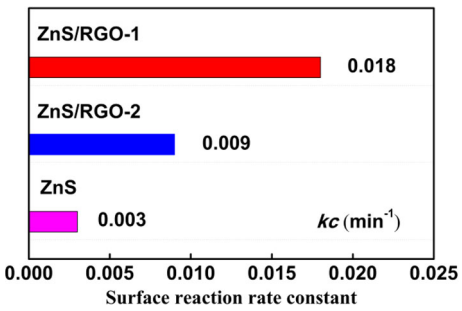

Fig. 6 Surface reaction rate constant of MB photodegradation in the presence of various catalysts under UV light irradiation (ZnSRGO-1 by sodium sulfide, ZnS/RGO-2 by thiourea)

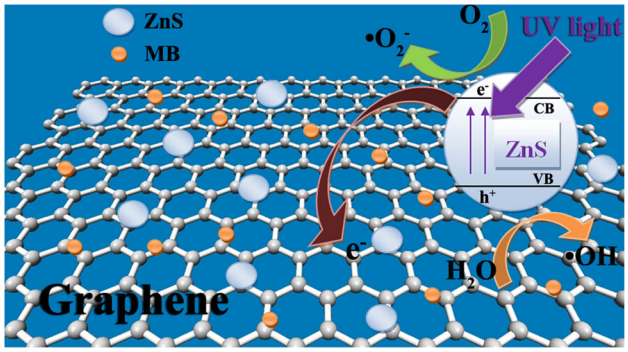

Fig. 7 MB photodegradation mechanism of MB by ZnS–RGO composites under UV light irradiation

semiconductor, the valence electrons of ZnS can be excited to the conduction band due to its narrow bandgap, which leaves behind a hole in the valance band by absorbing UV light. When the photo-generated electron–hole pair is migrated on the surface of the ZnS nanoparticles through the internal electric field of the semiconductor, the photo-generated electrons react with dissolved oxygen molecules and produce active oxygen radicals, and the photo-generated hole can react with the hydroxide ion derived from water to form hydroxyl radicals. These oxygen peroxide radicals and hydroxyl radicals may cause the oxidative decomposition of MB to CO_2, H_2O, and other mineralization products, which result in the degradation effect. It should be pointed out that although the UV radiation is also able to decompose some of the organic dyes directly, it could not affect the overall photocatalytic degradation efficiency owing to the low power of the UV light source adopted in the present study.

It was reported that the enhancement of the photocatalytic degradation properties of the ZnS/RGO nanocomposites can be attributed to two aspects [25–27]. One is that graphene possesses excellent conductivity owing to its two dimensional planar structure; thus, the rapid transport of photo-generated carriers could be achieved, and an effective charge separation is subsequently accomplished. The another is that graphene is capable of adsorbing organic dye molecules on the surface due to its great specific surface area with a large number of π–π conjugated double bonds. As a result, the ZnS/RGO nanocomposites generated the oxygen peroxide radicals and hydroxyl radicals which degraded the MB dye in the ultraviolet irradiation.

4 Conclusions

ZnS/RGO nanocomposites were successfully synthesized with GO aqueous solution as precursor, and $Na_2S{\cdot}9H_2O$ and $SC(NH_2)_2$ as S^{2-} donor, respectively. During the synthesis process, GO was reduced into RGO and ZnS

nanoparticles with a diameter of 5–10 nm were deposited on the surface of graphene sheets. The ZnS/RGO nanocomposite exhibits a significantly enhanced photocatalytic activity compared to pure ZnS, attributing to the efficient charge separation and the improved adsorption capacity on the surface of nanocomposite due to the introduction of graphene. The photocatalytic degradation efficiency of the nanocomposites prepared with $Na_2S{\cdot}9H_2O$ as S^{2-} donor was better than that of $SC(NH_2)_2$, because the former possesses higher hydrolysis rate than the latter, and the surface reaction rate constant of the former was two times higher than that of the latter and was six times higher than that of pure ZnS sample.

Acknowledgements The authors gratefully acknowledge the support of the program of Liaoning Education Department Nos. LG201605, Key Laboratory Open Fund of Shenyang Ligong University Nos. 4801004yb61-d, and the National Basic Research Program of China under Grant Nos. 2011CB932603 and the CAS/SAFEA International Partnership Program for Creative Research Teams.

References

1. O. Kozak, P. Praus, K. Koci, M. Klementova, J. Colloid Interf. Sci. **352**, 244–251 (2010)
2. D. Xiang, Y. Zhu, Z. He, Z. Liu, J. Luo, Mater. Res. Bull. **48**, 188–193 (2012)
3. G.Z. Shen, Y. Bando, D. Golberg, Appl. Phys. Lett. **88**, 1–3 (2006)
4. T. Hirakawa, P.V. Kamat, J. Am. Chem. Soc. **127**, 3928–3934 (2005)
5. V. Subramanian, E.E. Wolf, P.V. Kamat, J. Am. Chem. Soc. **126**, 4943–4950 (2004)
6. S.H. Elder, F.M. Cot, Y. Su, S.M. Heald, A.M. Tyryshkin, M.K. Bowman, Y. Gao, A.G. Joly, M.L. Balmer, A.C. Kolwaite, K.A. Magrini, D.M. Blake, J. Am. Chem. Soc. **122**, 5138–5146 (2000)
7. T. Tatsuma, S. Saitoh, P. Ngaotrakanwiwat, Y. Ohko, A. Fujishima, Langmuir **18**, 7777–7779 (2002)
8. A.M. Turek, I.E. Wachs, E. DeCanio, J. Phys. Chem. **96**, 5000–5007 (1992)
9. A.K. Geim, K.S. Novoselov, Nat. Mater. **6**, 183–191 (2007)
10. Y. Zhang, Y. Tan, H.L. Stormer, P. Kim, Nature **438**, 201–204 (2005)
11. K.I. Bolotin, K.J. Sikes, Z. Jiang, M. Klima, G. Fudenberg, J. Hone, P. Kim, H.L. Stormer, Solid State Commun. **146**, 351–355 (2008)
12. R.R. Nair, P. Blake, A.N. Grigorenko, K.S. Novoselov, T.J. Booth, T. Stauber, N.M.R. Peres, A.K. Geim, Science **320**, 1308 (2008)
13. Y.H. Zhang, N. Zhang, Z.R. Tang, Y.J. Xu, ACS Nano **6**, 9777–9789 (2012)
14. Y. Feng, N.N. Feng, G.Y. Zhang, G.X. Du, CrystEngComm **16**, 214–222 (2014)
15. C. Xu, X. Wang, J.W. Zhu, J. Phys. Chem. C **112**, 19841–19845 (2008)
16. Y. Lei, F.F. Cheng, R. Li, J. Xu, Appl. Surf. Sci. **308**, 206–210 (2014)
17. M. Sookhakiana, Y.M. Amina, W.J. Basirunb, Appl. Surf. Sci. **283**, 668–677 (2013)
18. F. Tuinstra, J.L. Koenig, J. Chem. Phys. **53**, 1126–1130 (1970)
19. T.N. Lambert, C.A. Chavez, B. Hernandez-Sanchez, P. Lu, N.S. Bell, A. Ambrosini, T. Friedman, T.J. Boyle, D.R. Wheeler, D.L. Huber, J. Phys. Chem. C **113**, 19812–19823 (2009)
20. S. Stankovich, D.A. Dikin, R.D. Piner, K.A. Kohlhaas, A. Kleinhammes, Y. Jia, Y. Wu, S.T. Nguyen, R.S. Ruoff, Carbon **45**, 1558–1565 (2007)
21. Q.H. Liang, Y. Shi, W.J. Ma, Z. Li, X.M. Yang, Phys. Chem. Chem. Phys. **14**, 15657–15665 (2012)
22. Q. Xiang, J. Yu, M. Jaroniec, Nanoscale **3**, 3670–3678 (2011)
23. Y. Li, X. Li, J. Li, J. Yin, Water Res. **40**, 1119–1126 (2006)
24. M. Ahmad, E. Ahmed, Z.L. Hong, J.F. Xu, N.R. Khalid, A. Elhissi, W. Ahmed, Appl. Surf. Sci. **274**, 273–281 (2013)
25. X.Q. An, J.C. Yu, RSC Adv. **1**, 1426–1434 (2011)
26. H. Zhang, X.J. Lv, Y.M. Li, Y. Wang, J.H. Li, ACS Nano **4**, 380–386 (2010)
27. J.S. Lee, K.H. You, C.B. Pack, Adv. Mater. **24**, 1084–1088 (2012)